Redox Biology 34 (2020) 101565

Contents lists available at ScienceDirect

Redox Biology

journal homepage: www.elsevier.com/locate/redox

A hydrogen peroxide responsive prodrug of Keap1-Nrf2 inhibitor for improving oral absorption and selective activation in inflammatory conditions

Mengchen Lu[a,b,1], Xian Zhang[a,1], Jing Zhao[a], Qidong You[a,b,**], Zhengyu Jiang[a,b,*]

[a] State Key Laboratory of Natural Medicines and Jiang Su Key Laboratory of Drug Design and Optimization, China Pharmaceutical University, Nanjing, 210009, China
[b] Department of Medicinal Chemistry, School of Pharmacy, China Pharmaceutical University, Nanjing, 210009, China

ARTICLE INFO

Keywords:
Keap1-Nrf2 pathway
Protein-protein interaction
H_2O_2
Prodrug
Inflammation
Oral administration

ABSTRACT

Transcription factor Nuclear factor erythroid 2-related factor 2 (Nrf2) and its negative regulator, the E3 ligase adaptor Kelch-like ECH-associated protein 1 (Keap1), control the redox and metabolic homeostasis and oxidative stress. Inhibitors of Keap1-Nrf2 interaction are promising in oxidative stress related inflammatory diseases but now hit hurdles. By utilizing thiazolidinone moiety to shield the key carboxyl pharmacophore in Keap1-Nrf2 inhibitor, a hydrogen peroxide (H_2O_2)-responsive prodrug **pro2** was developed. The prodrug modification improved the physicochemical properties and cell membrane permeability of the parent drug. **Pro2** was stable and stayed inactive under various physiological conditions, while became active by stimulation of H_2O_2 or inflammation derived reactive oxygen species. Moreover, **pro2** exhibited proper pharmacokinetic profile suitable for oral administration and enhanced anti-inflammatory efficiency *in vivo*. Thus, this novel prodrug approach may not only provide an important advance in the therapy of chronic inflammatory diseases with high level of H_2O_2, but also offer a fresh solution to improve the drug-like and selectivity issues of Keap1-Nrf2 inhibitors.

1. Introduction

Transcription factor nuclear factor erythroid 2-related factor 2 (Nrf2), as the master regulator of multiple cytoprotective responses, is pivotal in redox and metabolic homeostasis, as well as the regulation of oxidative stress [1,2]. Nrf2 activation enhances the anti-oxidant capacity and provides cryoprotection against oxidative stress and inflammatory insults [3,4]. Recently, therapeutic targeting of protein-protein interaction (PPI) of Nrf2 and its principal negative regulator, the E3 ligase adaptor Kelch-like ECH-associated protein 1 (Keap1) is emerging as a new strategy for drug development of chronic diseases [5–10]. Several types of PPI inhibitors with high potency in disrupting Keap1-Nrf2 interaction have been reported by both pharmaceutical companies and academic institutes [11–17]. However, concerns regarding pharmacokinetic properties and safety still remain. Most of the currently reported inhibitors are molecules with fairly high molecule weight and several polar functional groups [18–20], requirements for blocking the large and high polar Keap1-Nrf2 interface, and thus these compounds with high potency *in vitro* at present exhibit poor absorption, distribution, metabolism and excretion properties and relative low efficacy *in vivo*. Safety issues also challenge the further development of Keap1-Nrf2 inhibitors, since Nrf2 activation in normal cells can excessively strengthen the antioxidant system, resulting in the clearance of reactive oxygen species (ROS), which may disturb the pathological function of ROS [21]. Moreover, a concern about the increased cancer risk of Nrf2 activators also appears [22–25]. Somatic mutations in *KEAP1* and *NFE2L2*, resulting in high and unrestrained Nrf2 activity, have been regarded as driving factors of several tumors [26–28]. Therefore, the selective inhibition of Keap1-Nrf2 PPI in oxidative-stressed tissue is a key challenge, as it would dramatically benefit the therapeutic application. Designing a prodrug of Keap1-Nrf2 inhibitor that can reveal carboxyl acid group upon activation by ROS could kill two birds with one stone. It can not only improve the poor pharmacokinetic properties caused by the polar and ionizable characters of

* Corresponding author. State Key Laboratory of Natural Medicines and Jiang Su Key Laboratory of Drug Design and Optimization, China Pharmaceutical University, Nanjing, 210009, China.
** Corresponding author. State Key Laboratory of Natural Medicines and Jiang Su Key Laboratory of Drug Design and Optimization, China Pharmaceutical University, Nanjing, 210009, China.
E-mail addresses: youqd@163.com (Q. You), jiangzhengyucpu@163.com (Z. Jiang).
[1] These authors contributed equally.

https://doi.org/10.1016/j.redox.2020.101565
Received 26 March 2020; Received in revised form 22 April 2020; Accepted 29 April 2020
Available online 11 May 2020

carboxyl acid group, but also shield the key group of Keap1-binding until reaching the target cells, specifically rebalancing the redox state in pathological cells while not affecting normal cells.

Hydrogen peroxide (H_2O_2), an uncharged molecule and a stable ROS, is endogenously produced and ubiquitous existed in living organisms [29,30]. Physiologically, H_2O_2 plays an active role in redox signaling through reversible redox post-translational modifications, and its level is fine-tuned by anti-oxidant system [31–33]. Nevertheless, high level of H_2O_2 has been closely associated with several pathological conditions, including inflammation [34], neurodegenerative disorders [35] and cancer [36]. On one hand, H_2O_2 overabundance, together with the aberrant oxidative stress, contributes to the pathology of these conditions. On the other hand, excessive level of H_2O_2 in pathological microenvironments could be an ideal trigger for targeting activation of therapeutic agents [37]. Chang's group reported the pioneer work of H_2O_2-responsive aryl boronate trigger [38,39], inspiring the rapid development of aryl boronate-based probes of H_2O_2 [40–45]. Using aryboronates or boronic acids as the trigger units, Peng's group developed the first H_2O_2-activated DNA cross-linking agents [46], and various H_2O_2-activated anti-cancer agents have been identified [47–53].

More recently, increasing evidence from different studies supports the relation between oxidative stress and the pathogenesis of inflammation, and it inspired the research around the H_2O_2-responsive cytoprotective and anti-inflammation agents, including prodrugs of methotrexate and aminopterin for the treatment of rheumatoid arthritis [54,55], prodrugs of H_2S donors [56,57] and CO donors [58], and prodrug of angiogenin for neuroprotective activity [59]. The presence of high level of H_2O_2 in inflammatory conditions also provides an ideal trigger for the selective activation of Nrf2. To the best of our knowledge, an oral H_2O_2-responsive prodrug for Nrf2 activation is still unavailable, which limits therapeutic usage of Nrf2 activation agents in chronic inflammatory diseases. It is therefore envisioned that improvements could be made to develop new orally administered H_2O_2-responsive prodrug of Keap1-Nrf2 PPI inhibitors.

Here, we report a H_2O_2-reponsive prodrug of Keap1-Nrf2 inhibitor by shielding the key carboxyl pharmacophore with the H_2O_2-sensitive thiazolidinone moiety. Our study showed that prodrug modification of the parent drug can improve the drug-like properties and enable the molecule suitable for oral administration. We proved that the caged inhibitor lost its activity in disrupting Keap1-Nrf2 interaction and inflammation derived ROS allowed for the release of the active entity to antagonize the inflammatory conditions in both cellular and *in vivo* inflammatory models. To the best of our knowledge, it is the first example of H_2O_2-responsive prodrug suitable for oral administration, and this study highly stresses the *in vivo* anti-inflammation efficacy of small molecule Keap1-Nrf2 inhibitory agents.

2. Materials and methods

2.1. Chemistry

The synthesis of prodrugs is highlighted in Scheme 1. All chemicals purchased from commercial suppliers were used as received unless otherwise stated. All solvents were reagent grade and, when necessary, were purified and dried by standard methods. Reactions were monitored by thin-layer chromatography on silica gel plates (GF-254) visualized under UV light. Melting points were determined on a MelTEMP II melting point apparatus without correction. ^{1}H NMR and ^{13}CNMR spectra were recorded in $CDCl_3$ or DMSO-d_6 on a Bruker Avance-300 instrument. Chemical shifts (δ) are reported in parts per million (ppm) from tetramethyl silane (TMS) using the residual solvent resonance ($CDCl_3$: 7.26 ppm for ^{1}H NMR, 77.16 ppm for ^{13}C NMR; DMSO: 2.5 ppm for ^{1}H NMR, 39.5 ppm for ^{13}C NMR). Multiplicities are abbreviated as follows: s = singlet, d = doublet, t = triplet, q = quartet, m = multiplet). HR-MS spectra were recorded on a Water Q-Tof micro mass spectrometer. Flash column chromatography was performed with 100–200 mesh silica gel and yields refer to chromatographically and spectroscopically pure compounds. The purity (≥95%) of the compounds was verified by the HPLC study performed on an Agilent C18 (4.6 mm × 150 mm, 3.5 μm) column using a mixture of solvent methanol/water at a flow rate of 0.5 mL/min and monitored by UV absorption at 254 nm. The petroleum ether used in the study was the grade of analytical pure and boiled over the range 60–90 °C.

N,N'-(naphthalene-1,4-diyl)bis(4-methoxy-N-(2-oxo-2-(2-oxothiazolidin-3-yl)ethyl) benzenesulfonamide) ***(pro1)*** To a solution of **1** (0.5 g, 0.81 mmol) in DMF (10 mL) was added DCC (0.37 g, 1.79 mmol) and DMAP (0.22 g, 1.79 mmol), stirring at room temperature. After 30 min, thiazolidin-2-one (0.37 g, 3.60 mmol) was added and the mixture was stirred overnight. After reaction finished, the mixture was poured onto water and extracted with Et_2O (3 × 20 mL). The organic extracts were combined, dried over Na_2SO_4, and concentrated in vacuo. The crude product was purified by column chromatography to give the pure product as a white solid (0.368 g, 58%). R_f = 0.42 (EA/PE 1:1); m.p. 234–235 °C; ^{1}H NMR (300 MHz, DMSO-d_6) δ 8.28 (dd, J = 6.9, 3.4 Hz, 2H; Ar–H), 7.57 (d, J = 8.5 Hz, 4H; Ar–H), 7.10 (d, J = 8.8 Hz, 4H; Ar–H), 7.03 (d, J = 8.5 Hz, 4H; Ar–H), 4.23 (s, 4H; CH_2), 3.87 (s, 6H; OCH_3), 3.81 (s, 4H; CH_2). 3.01–3.06 (t, J = 7.1 Hz, 4H; CH_2); ^{13}C NMR (75 MHz, Chloroform-*d*) δ 173.57, 168.62, 163.32, 134.73, 132.71, 130.29, 128.91, 127.26, 124.77, 121.74, 114.44, 56.89, 55.81, 46.72, 26.03; HRMS (ESI): *m/z* calcd. for $C_{34}H_{32}N_4O_{10}S_4+H^+$: 785.1074 $[M+H]^+$, found: 785.1074.

4-methoxy-N-(4-((4-methoxyphenyl)sulfonamido)naphthalen-1-yl)-N-(2-oxo-2-(2-oxothiazolidin-3-yl)ethyl)benzenesulfonamide ***(pro2)*** To a solution of **2** (0.5 g, 0.90 mmol) in DMF (10 mL) was added DCC (0.41 g, 1.98 mmol) and DMAP (0.24 g, 1.98 mmol), stirring at room temperature. After 30 min, thiazolidin-2-one (0.186 g, 1.80 mmol) was added and the mixture was stirred overnight. After reaction finished, the mixture was poured onto water and extracted with Et_2O (3 × 20 mL). The organic extracts were combined, dried over Na_2SO_4, and concentrated in vacuo. The crude product was purified by column chromatography to give the pure product **pro2** as a white solid (0.263 g, 46%).R_f = 0.31 (EA/PE 1:1); m.p. 229–230 °C; ^{1}H NMR (300 MHz, DMSO-d_6): δ = 10.23 (s, 1H; NH), 8.03 (d, J = 8.6 Hz, 2H; Ar–H), 7.65 (d, J = 8.5 Hz, 2H; Ar–H), 7.49 (d, J = 8.8 Hz, 4H; Ar–H), 7.07 (dd, J = 21.6, 8.4 Hz, 6H; Ar–H), 5.00–4.77 (m, 4H; CH_2), 3.95 (s, 2H; CH_2), 3.86–3.75 (m, 6H; OCH_3); ^{13}C NMR (75 MHz, Chloroform-*d*) δ 173.40, 168.46, 163.24, 163.15, 134.57, 132.61, 132.54, 130.83, 130.38, 130.12, 129.54, 129.19, 128.74, 127.26, 127.09, 124.61, 121.57, 120.51, 114.27, 113.92, 56.72, 55.64, 46.55, 25.86; HRMS (ESI): *m/z* calcd. for $C_{29}H_{27}N_3O_8S_3+NH_4^+$: 659.1299 $[M + NH_4]^+$; found: 659.1300.

2.2. Biology

2.2.1. HPLC assay for drug release study

Compounds were dissolved in DMSO as solutions (10 mM) and stored at −20 °C. The incubation was initiated by the addition of compound (10 mM) to phosphate buffer solution (PBS) (10 mM, pH 7.4) to obtain a final concentration of 50 μM and then added H_2O_2 followed by vortex mixing. The solution was incubated at 37 °C and conducted in triplicate. Samples were taken at appropriate time intervals and directly analyzed by HPLC analysis. Peak areas were recorded to calculate the percentage of compounds. Agilent 1260 HPLC and DAD detector with conditions: Agilent C18 column (4.6 × 150 mm, 3.5 μm); Mobile phase: methanol 70%; Flow rate: 0.5 mL/min. A standard curve for compounds was made to fit the measured concentrations.

2.2.2. Physicochemical property and cell membrane permeability determination

The pKa and partition coefficient (log D, pH 7.4) were determined according to the methods of Avdeef and Tsinman on a Gemini Profiler instrument (pION) by the “gold standard” Avdeef−Bucher

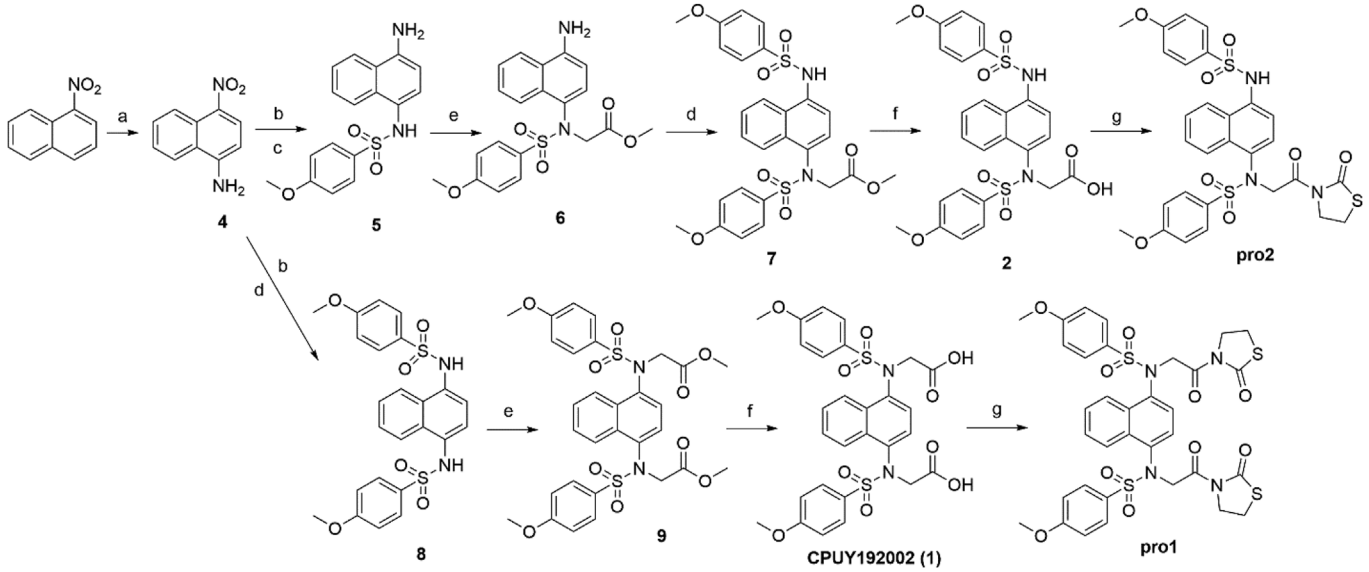

Scheme 1. Reagents and conditions: (a) $NH_2OH{\cdot}HCl$, 95% ethanol, MeOH, 60 °C, 2 h, yield 57%; (b) Pd/C, H_2, THF, rt, 4 h; (c) 4-Methoxybenzenesulfonyl chloride, Na_2CO_3, THF, 0 °C, 2 h, yield 83%; (d) 4-Methoxybenzenesulfonyl chloride, toluene, pyridine, 100 °C, 2 h, yield 64%; (e) DMF, K_2CO_3, ethyl bromoacetate, rt, 3 h, yield 84%; (f) LiOH, MeOH, H_2O, 2 h, yield 94%; (g) thiazolidin-2-one, DMAP, DCC, DMF, rt, 6 h, yield 76%.

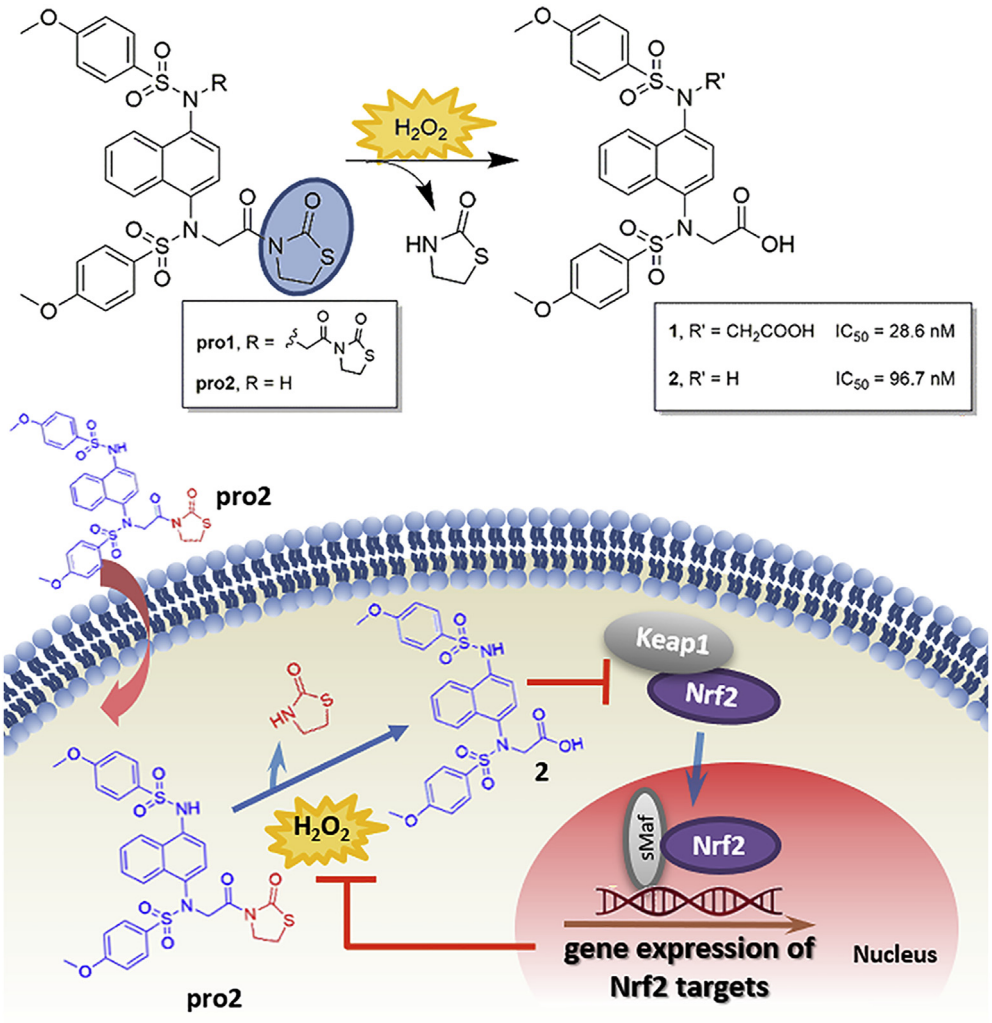

Fig. 1. Proposed scheme for activation of the thiazolidinone prodrugs.

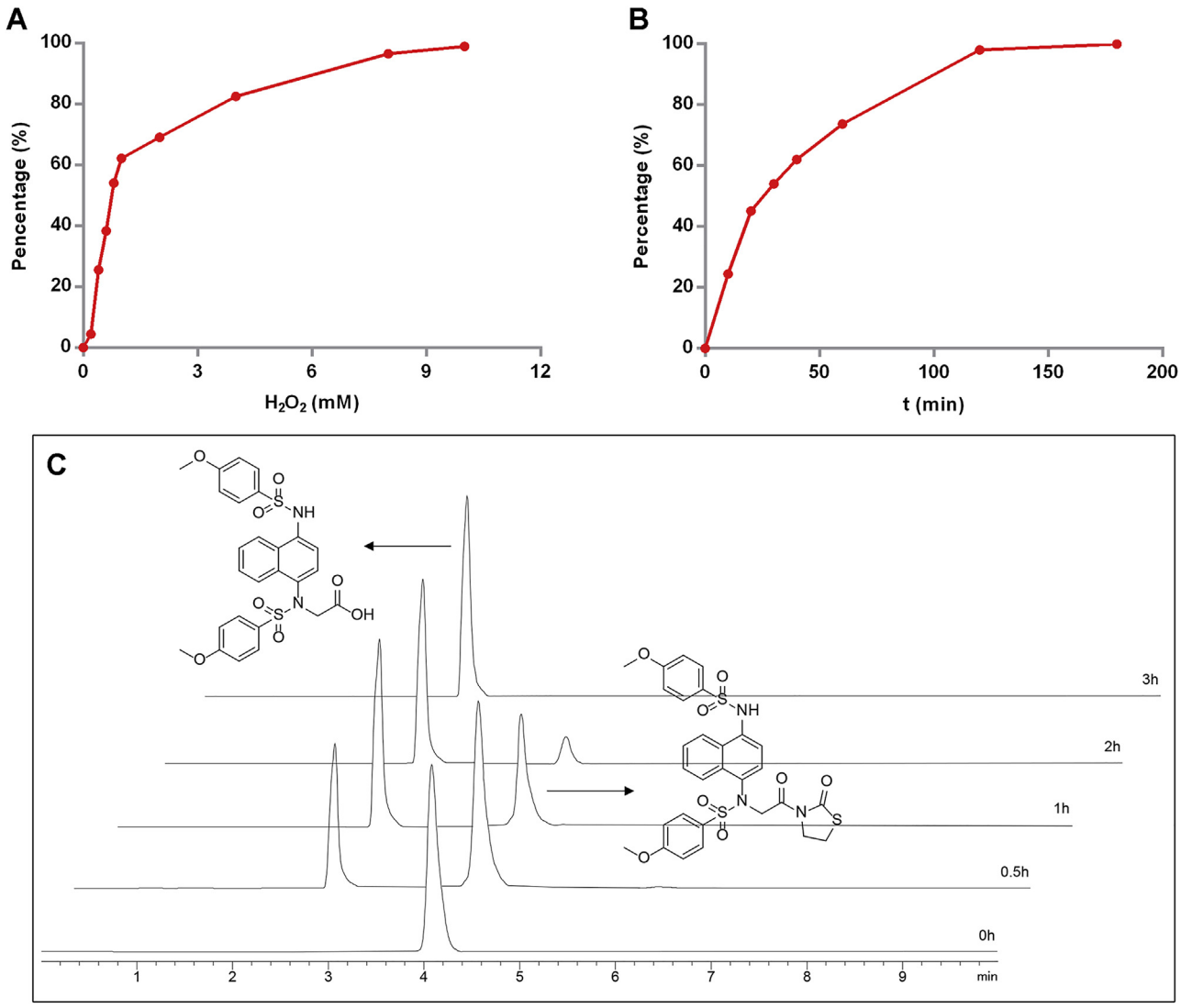

Fig. 2. Activation of **pro2** with H_2O_2. (A) Activation of **pro2** under different concentrations of H_2O_2 after incubating 24 h. (B) Time release curve of **pro2** with 10 mM H_2O_2. (C) HPLC chromatograms of the activation of **pro2** by H_2O_2.

potentiometric titration method. The pH-metric method was used to determine the intrinsic solubility. The potentiometric solubility data were obtained with the pSOL model 3 instrument (pION INC., Cambridge, MA, USA). Permeability coefficients were determined via double sink PAMPA on a PAMPA Explorer instrument (pION).

2.2.3. Cell culture and ARE-luciferase activity assay

The mouse RAW 264.7 cell line was obtained from Cell Bank of Shanghai Institute of Biochemistry and Cell Biology, Shanghai Institutes for Biological Sciences, Chinese Academy of Sciences. HepG2 cells stably transfected with a luciferase reporter (HepG2-ARE-C8) were kindly provided by Professor Dr. A. N. Tony Kong (Rutgers University, Piscataway, NJ) and Prof. Rong Hu (China Pharmaceutical University, Nanjing). The cells were maintained by regular passage in modified RPMI-1640 medium (GiBco, Invitrogen Corp., USA) supplied with 10% FBS, 100 units per mL penicillin and 100 μg/mL streptomycin, cultured at 37 ˚C in a water vapour saturated atmosphere with 5% CO_2. The experimental procedures were carried out as reported previously [60].

2.2.4. RNA extraction and qRT-PCR analysis

The experimental procedure of quantitative real-time RT-PCR was previously reported. Total RNA of RAW264.7 cells was extracted from the treated cells using TRIzol reagent (Invitrogen). Then the RNA was converted to cDNA by reverse transcriptase (PrimeScript RT reagent kit) according to the manufacturer's instructions. Quantitative real-time RT-PCR analysis of Nrf2, HO-1, NQO1 and GCLM were performed by using the StepOne System Fast Real Time PCR system (Applied Biosystems). The values are expressed as the fold of the control. All genes' mRNA expression was normalized against β-Actin expression.

2.2.5. Western blot analysis

Anti-Nrf2 (ab62352), anti-IL-1β (ab45692) antibodies were purchased from Abcam Technology (Abcam Technology, England). Anti–HO–1 (SC-136960) and anti-NQO1 (SC-271116) antibodies were purchased from Santa Cruz Biotechnology (Santa Cruz, CA, USA). Anti-β-actin (60,008-1-lg), anti-GCLM (14241-1-AP) antibodies were purchased from Proteintech Group (Proteintech Group, USA). Briefly, the extracts were separated by SDS-PAGE and then electro-transferred to PVDF membranes (PerkinElmer, Northwalk, CT, USA). Membranes were blocked with 1% BSA for 1 h followed by incubation with a primary antibody at 4 ˚C overnight. Then they were washed and treated with a DyLight 800 labeled secondary antibody at 37 ˚C for 2 h. The membranes were screened through the odyssey infrared imaging System (LI-COR, Lincoln, Nebraska, USA).

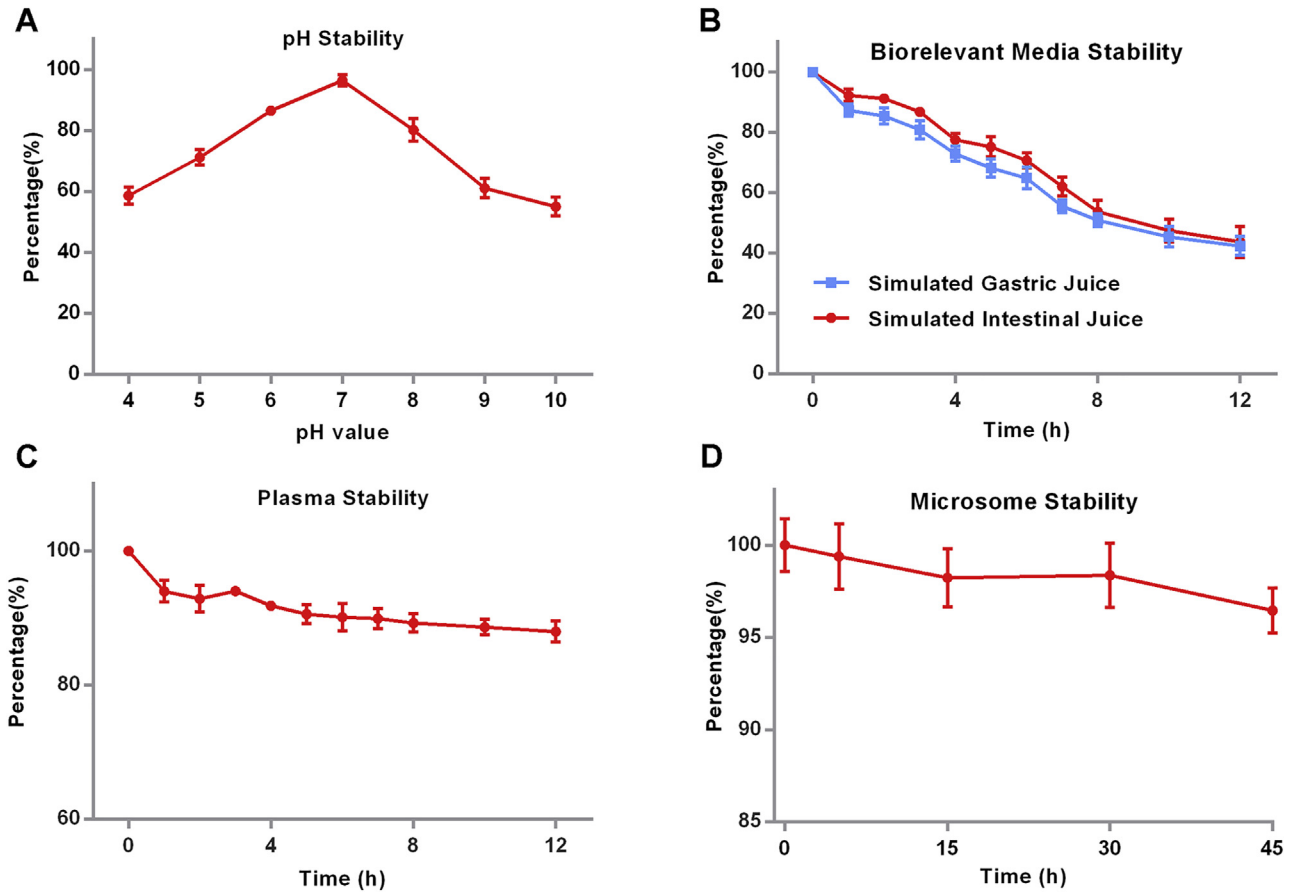

Fig. 3. Stability of the prodrug **pro2**. Stability of **pro2** (20 μM) in different relevant physiological conditions including different pH (4–10) (A), SGF (B), SIF (B), rat plasma (C) and liver microsomes (D).

Table 1
Physicochemical property and membrane permeability measurement.

Compd	pKa	LogD at pH 7.4	Aqueous solubility at pH 7.4 (μg/mL)	Pe at pH 7.4 (10 − 6 cm/s)
Pro2	4.53	2.34	879.6	6.35
2	4.31	1.88	428.2	0.80

2.2.6. IL-1β, IL-18, IL-6, TNF-α and NO production

Levels of IL-1β (IL-1β (m) ELISA kit, EK0394, Boster), IL-18 (IL-18 (m) ELISA kit, #EMC011, NeoBioscience), IL-6 (IL-6 (m) ELISA kit, EK0411, Boster), TNF-α (TNF-α (m) ELISA kit, EK0527, Boster) and NO production (Nitrate/Nitrite Assay Kit, S0023, Beyotime, China) were evaluated using commercially available kits according to the manufacturer's instructions.

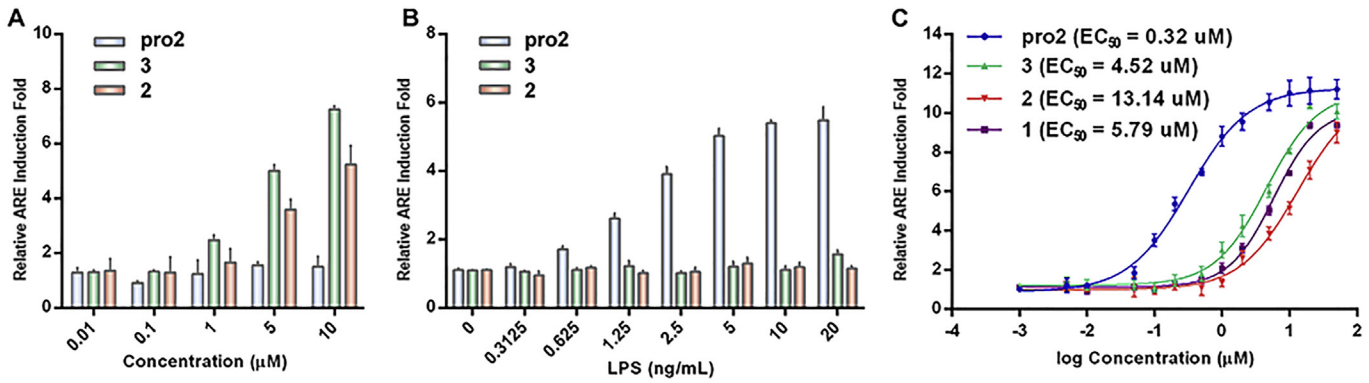

Fig. 4. Comparison of activities of **pro2**, **2** and **3**. (A) Relative ARE induction activity in HepG2-ARE-C8 cells under normal conditions. (B) Relative ARE induction activity under various concentrations of LPS in HepG2-ARE-C8 cells. Cells were pretreated by various concentrations of LPS for 8 h, and then treated with selected compounds (200 nM) or DMSO (for use as the control) for another 12 h. The values are expressed as the fold of the control. (C) The EC_{50} curves of the relative ARE induction activity. Cells were pretreated by LPS (20 ng/mL) for 8 h, and then treated with various concentrations (0.001–50 μM) of selected compounds or DMSO (for use as the control) for another 12 h. The values are expressed as the fold of the control.

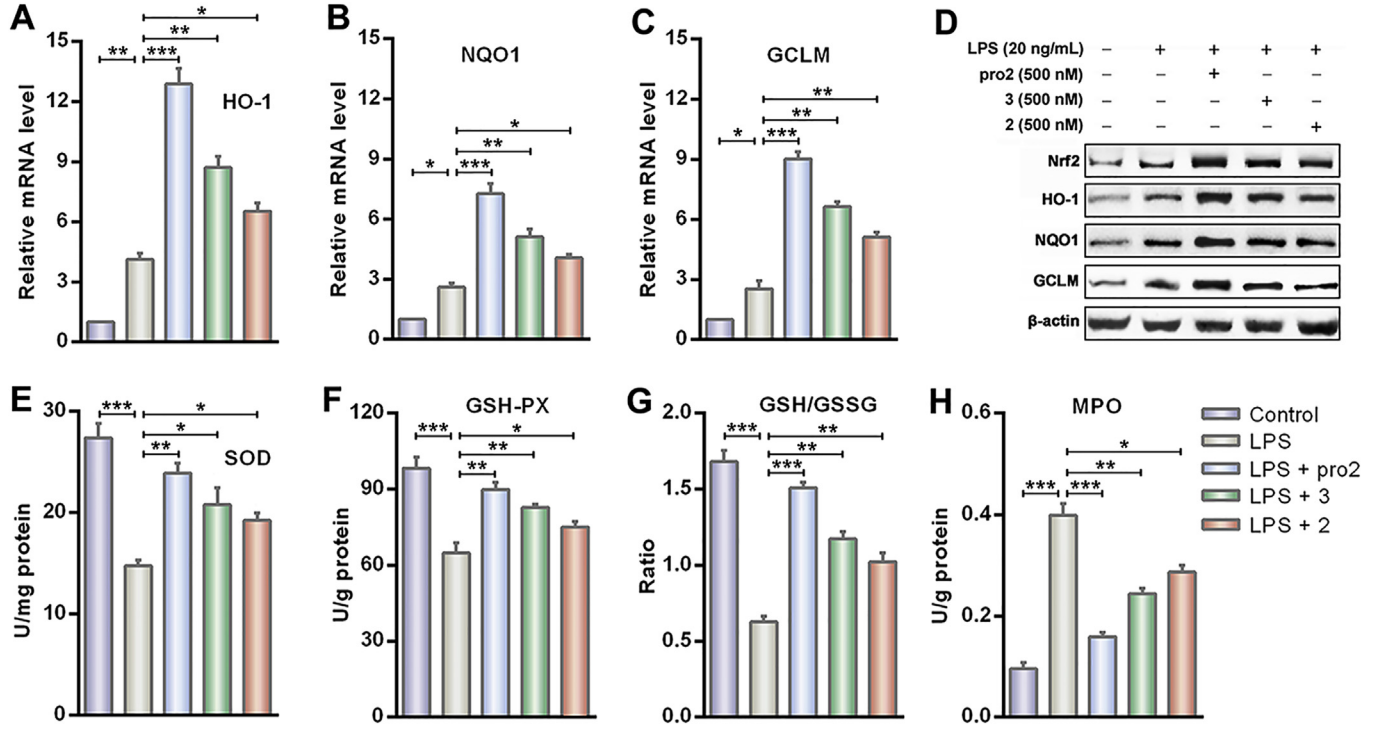

Fig. 5. Prodrug activated the Nrf2-ARE regulated antioxidant system in the RAW264.7 cells. RAW264.7 cells were pretreated with 20 ng/mL LPS for 8 h and then treated with compounds for another 16 h. PCR analysis of HO-1 (A), NQO1 (B) and GCLM (C) in the RAW264.7 cells. (D) Western blot analysis of the Nrf2-targeted proteins in the RAW264.7 cells. (E–H) Measurement of SOD, GSH-PX, GSH/GSSG and MPO level in the RAW264.7 cells. The values shown are the means ± SEM (n = 3 independent observations). *p < 0.05, **p < 0.01, ***p < 0.001, which were calculated with one-way ANOVA.

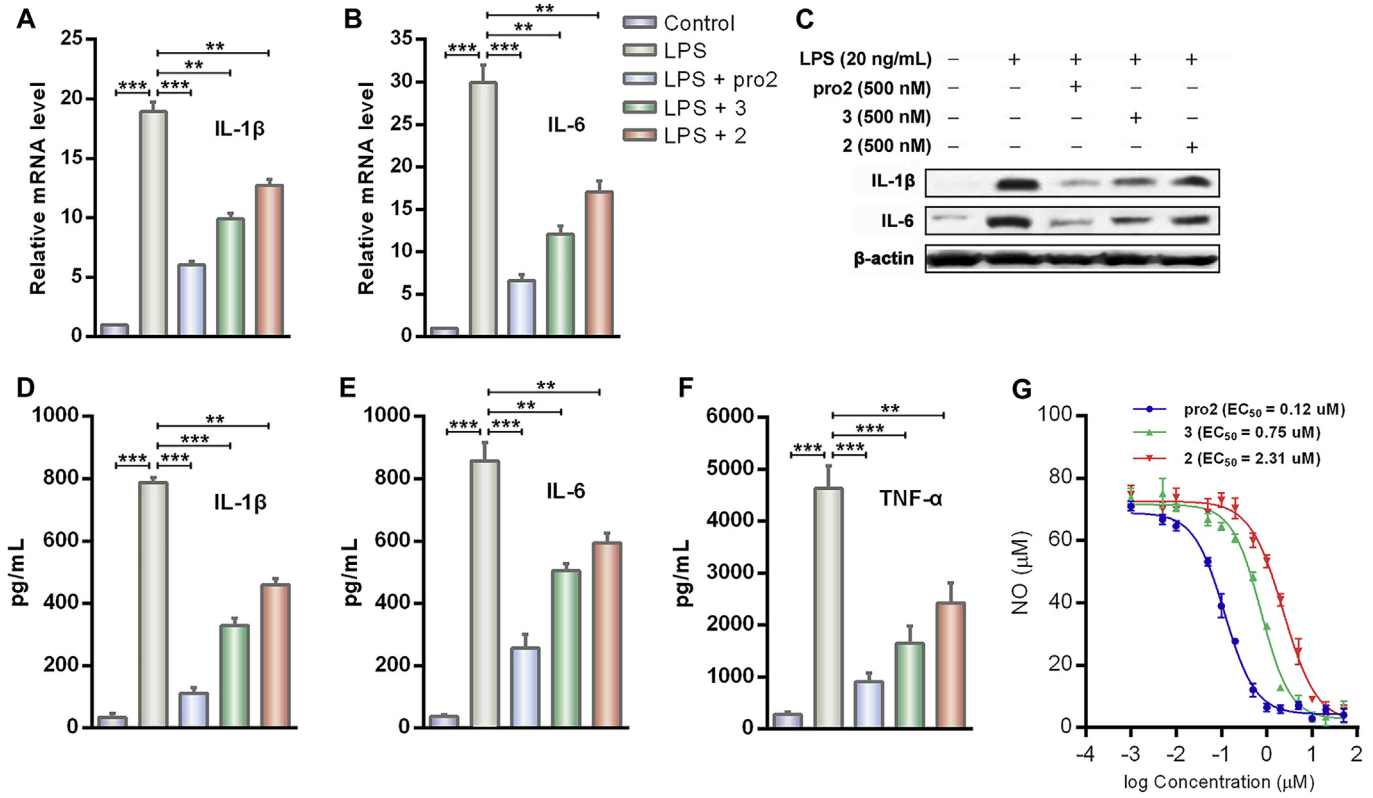

Fig. 6. Prodrug reduced inflammatory factors production induced by LPS in the RAW264.7 cells. RAW264.7 cells were pretreated with 20 ng/mL LPS for 8 h and then treated with compounds for another 16 h. PCR analysis of IL-1β (A) and IL-6 (B) in the RAW264.7 cells. (C) Western blot analysis of IL-1β and IL-6 protein levels in the RAW264.7 cells. Concentrations of IL-1β (D), IL-6 (E), TNF-α (F) and NO (G) in the RAW264.7 cell culture supernatants. The values shown are the means ± SEM (n = 3 independent observations). *p < 0.05, **p < 0.01, ***p < 0.001, which were calculated with one-way ANOVA.

Table 2
Physicochemical Properties *in vivo*.

	P.O. (10 mg/kg)	*I.V.* (2 mg/kg)
$T_{1/2}$ (hr)	2.09 ± 0.93	4.41 ± 3.01
T_{max} (hr)	0.67 ± 0.29	–
C_{max} (ng/mL)	2753 ± 15.3	–
AUC_{0-t} (ng·hr/mL)	6203 ± 248	1842 ± 363
$AUC_{0-\infty}$ (ng·hr/mL)	6315 ± 273	1854 ± 366
Vz_F(L/kg)	4.79 ± 2.17	6.44 ± 4.09
Cl_F (mL/min/kg)	26.4 ± 1.14	18.5 ± 3.9
MRT (hr)	1.82 ± 0.35	1.25 ± 0.30

Bioavailability 68.1%.

2.2.7. Stability

(1) pH Stability. PBS buffers with different pH values (pH 4–10) were to prepare by using 0.1 M HCl solution and 0.1 M NaOH solution. The prodrug **pro2** (20 μM) was co-incubated with PBS buffer with different pH values at 37 °C and the assays were conducted in triplicate. After 24 h incubation, solution was filtered and adopted in direct injection analysis by HPLC. The injections were proceeded thrice, and peak areas were recorded to calculate the percentage of compounds;

(2) Plasma stability. Sample of prodrug **pro2** (20 μM) was co-incubated with mice plasma at 37 °C for different times and three parallel experiments was conducted. Protein was precipitated by adding methanol and samples were subjected to vortex mixing and then centrifugation for 5 min at 12,000 rpm to deproteinize. Samples of the resulting supernatants were withdrawn and analyzed by HPLC to record peak areas;

(3) Microsome stability. The *in vitro* microsome stability of the compound was evaluated in isolated liver microsomes (from CD-1 male rat). Ketanserin was used as reference compounds. A solution of liver microsomes (20 mg/mL) was added to a microcentrifuge tube containing of PBS at 37 °C, and the mixture was shaken for 10 min before the actual assay was started. Then, a DMSO solution of test compound (0.5 mM) was added. For 0 min, add ice-cold acetonitrile to the wells of 0 min plate and then add NADPH stock solution (6 mM). Pre-incubate all other plates at 37 °C for 5 min. Add NADPH stock solution (6 mM) to the plates to start the reaction and timing. At 5 min, 15 min, 30 min, and 45 min, add ice-cold acetonitrile to the wells of corresponding plates, respectively, to stop the reaction. After quenching, shake the plates at the vibrator for 10 min and then centrifuge at 5000 rpm for 15 min. Transfer the supernatant from each well into a 96-well sample plate containing ultra pure water for LC-MS/MS analysis;

(4) Stability in artificial gastric juice and intestinal juice. Artificial gastric juice and intestinal juice were purchased from commercial suppliers. Sample of **pro2** (20 μM) was co-incubated with artificial gastric juice and intestinal juice respectively for different times at 37 °C and three parallel experiments was conducted. Zymoprotein was precipitated by adding methanol and samples were subjected to vortex mixing and then centrifugation for 5 min at 5000 rpm. Samples of the resulting supernatants were withdrawn and analyzed by HPLC to record peak areas; All the chromatographic condition is consistent with above-mentioned.

2.2.8. LPS challenge mouse acute inflammation model

Animal studies were conducted according to protocols approved by Institutional Animal Care and Use Committee of China Pharmaceutical University. All animals were appropriately used in a scientifically valid and ethical manner. After treatment with regular drinking water for 2 days for adaptation, female C57BL/6 mice (6–8 weeks of age, weighing 18–20 g) were randomized into eight groups: (A) Control group (n = 3); (B) LPS (Sigma-Aldrich, St. Louis, no. L4130) model group (300 μg/kg/day, n = 8); (C) LPS (300 μg/kg/day) + **pro2** low-dose (10 mg/kg/day) group (n = 8); (D) LPS (300 μg/kg/day) + **pro2** high-dose (40 mg/kg/day) group (n = 8); (E) LPS (300 μg/kg/day) + parent compound **2** high-dose (40 mg/kg/day) group (n = 8); (F) LPS (300 μg/kg/day) + dexamethasone low-dose (10 mg/kg/day) group (n = 8); (G) **pro2** high-dose (40 mg/kg/day) group (n = 3); (H) parent compound **2** high-dose (40 mg/kg/day) group (n = 3).

Animals in control and (G, H) groups received a single IP injection containing 500 μL of saline (day −3, −2, −1). All LPS-challenged mice received a single IP injection containing 500 μL of LPS (day −3, −2, −1). Four hours after the injection, mice were pretreated with compound (ig, in 500 μL of saline, day −3, −2, −1). Animals were sacrificed 24 h after the last dose of compound and sera were collected (day 0). The level of the cytokines in sera was measured using ELISA kits.

3. Results and discussion

3.1. Design and synthesis of prodrugs

Previously, our group reported **CPUY192002 (1)**, the first nanomole Keap1-Nrf2 inhibitor bearing two carboxylic acid groups important for the Keap1 binding [61], and further study showed that removal of one of the carboxylic acid groups induced moderate decrease in activity from an IC_{50} of 28.6 nM–96.7 nM (compound **2**, Fig. S1) in the fluorescence polarization (FP) competition assay, which has also been confirmed by the study of Moore's group [62]. However, for both of the two inhibitors, micromole range concentrations are needed for achieving obvious Nrf2 activation effects in various cellular models [62–64]. The offset between the *in vitro* potency and cellular activities may largely attribute to the poor permeability caused by the ionizable carboxyl group. Thus, we chose to develop a ROS-responsive prodrug by appending a ROS-cleavable protecting group to the carboxylic acid moiety. The pioneer work from Cohen et al. reported the first identified thiazolidinone protecting group that can reveal carboxyl acid moiety upon activation by H_2O_2 [65]. Compared to the widely used aryl boronic esters trigger, the promising characters of low molecular mass and no GSH deletion byproducts make the thiazolidinone-based trigger more suitable for developing anti-oxidant and anti-inflammation

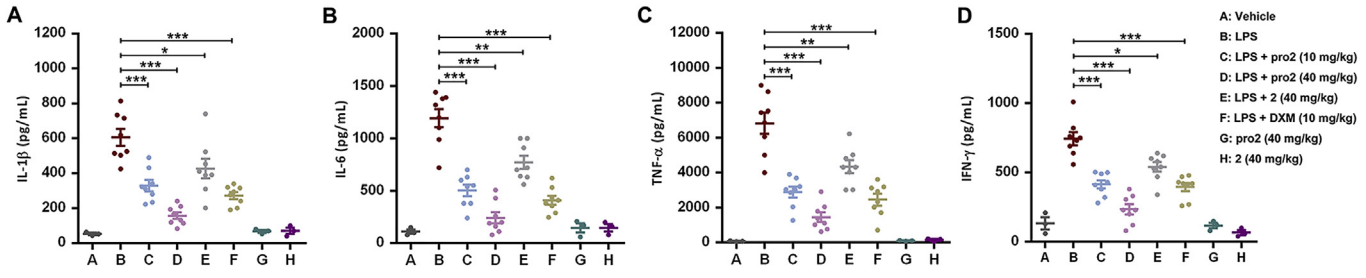

Fig. 7. Prodrug reduced the LPS-induced production of the pro-inflammatory factors *in vivo*. Levels of serum IL-1β (A), IL-6 (B), TNF-α (C) and IFN-γ (D) were measured by Elisa kits. *p < 0.05, **p < 0.01, ***p < 0.001, which were calculated with one-way ANOVA.

agents. With these considerations in mind, we designed and synthesized the thiazolidinone-based prodrugs of potent Keap1-Nrf2 inhibitors (**pro1** and **pro2**, Fig. 1 and Scheme 1). These two prodrugs demonstrated no inhibition against Keap-Nrf2 interaction in the FP assay, indicating that the thiazolidinone promoiety did abolish the activity of parent drugs.

The synthesis of the prodrugs is shown in Scheme 1. Amination of commercially available 1-nitronaphthalene afforded 4-Nitronaphthalen-1-amine (**4**). The nitro group of **4** was reduced by hydrogen and Pd/C, and the subsequent condensation with 4-Methoxybenzenesulfonyl chloride gave compound **5**. Compound **6** were obtained by nucleophilic substitution of NH by ethyl bromoacetate in the presence of K_2CO_3 in DMF, and the subsequent condensation with 4-Methoxybenzenesulfonyl chloride gave compound **7**. Hydrolysis of the ester group of **7** resulted in the parent compound **2**. The thiazolidinone moiety was then introduced through a DCC/DMAP-mediated coupling with **2** to give the desired prodrug **pro2**. The synthesis for **CPUY192002 (1)** had been previously reported [61]. Amide bond formation between the carboxylic acid compound **1** and the thiazolidinone promoiety was also performed via addition of DCC and DMAP in DMF, which finally gave the prodrug **pro1**.

3.2. Validation of H_2O_2-responsive parent drug release and evaluation of stability

To verify that H_2O_2 was able to deprotect the thiazolidinone group, H_2O_2-induced prodrug transformation experiments were performed and monitored by HPLC. However, in the presence of H_2O_2, the prodrug **pro1**, which contains two thiazolidinone pro-moieties, was hydrolyzed to generate the compound with only one free carboxylic acid, identified by UPLC/HRMS, and the production of compound **1** cannot be observed even after 12 h (Fig. S2). In the case of the prodrug **pro2**, as expected, after incubating 24 h, a H_2O_2 concentration-dependent release of the parent compound **2** was observed, and approximately 60% prodrug can be released upon treatment with 1 mM H_2O_2 (Fig. 2A). Upon treatment with 10 mM H_2O_2, **pro2** was activated with increasing incubating time and completely released to the parent compound **2** within 3 h (> 98% conversion determined by HPLC, Fig. 2B and C). Then, the H_2O_2-responsive activation of **pro2** was further examined in live cells. Murine macrophage cells (RAW264.7) were stimulated with H_2O_2 for 24 h to induce the intracellular ROS and then culture medium was replaced with fresh medium. **Pro2** (1 mM) was added to stimulated or non-stimulated cells for incubation and the cell lysates were analyzed by LC-MS. No peak of **2** was observed in non-stimulated cells, while obvious signal of **2** appeared in stimulated cell lysate (Fig. S3). The results demonstrated that **pro2** can be taken up by cells and transformed to **2** by intracellular H_2O_2.

Then, the stability of the synthesized prodrug was evaluated in different relevant physiological conditions. It was observed that **pro2** was relatively stable to hydrolysis in PBS of different pH values from 4 to 10 after incubating 24 h (Fig. 3A). In bio-relevant media, including simulated gastric fluid (SGF) and simulated intestinal fluid (SIF), more than 50% of **pro2** remained after 8 h (Fig. 3B). Moreover, **pro2** is quite stable in rat plasma (Fig. 3C) and in co-incubation with rat liver microsomes (Fig. 3D), indicating the high metabolic stability.

3.3. Physicochemical properties and cell membrane permeability

Then, we determined the physicochemical properties of **pro2** as well as the parent compound **2**. As shown in Table 1, the pKa and log $D_{pH=7.4}$ of **2** are 4.31 and 1.88, while the pKa and log$D_{pH=7.4}$ of **pro2** are 4.53 and 2.34, respectively. These results confirmed that **pro2** is a less ionizable and less polar molecule than **2**, which can enhance the passive cell membrane permeability of **pro2**. We then examined the cell membrane permeability by using a standard parallel artificial membrane permeability assay (PAMPA). The parent compound **2** showed a permeability coefficients (Pe) value of 0.80×10^{-6} cm/s, while **pro2** gave a *Pe* value of 6.35×10^{-6} cm/s, which proved that **pro2** can permeate the cell membrane more easily.

3.4. Selective activation of prodrug by inflammation-derived ROS

Next, the cellular biological activity of **pro2** was investigated. Initial studies aimed at demonstrating selective Nrf2 activation effects of **pro2** upon ROS. The Nrf2/ARE luciferase reporter assay was applied to evaluate the cellular Nrf2 activity, and the methyl ester prodrug **3**, which is not responsive to cellular ROS, was used as an unselective control to demonstrate the ROS-responsive selectivity of **pro2**. As shown in Fig. 4A, both of **2** and **3** concentration-dependently induced the ARE activity. The methyl ester prodrug **3** showed higher ARE-induction activity compared to the active compound **2**. However, **pro2** kept nearly inactive even at the highest concentration, which indicated that **pro2** is stable and does not affect the Nrf2-ARE system under physiological conditions. In order to simulate the inflammation related high ROS microenvironment, cells were exposed to lipopolysaccharide (LPS), a widely used inflammation inducer which can enhance the production of intracellular ROS. Treatment with LPS can elevate ROS level with the increase of LPS concentration (Fig. S4). Then, Nrf2-ARE induction activites of these compounds were examied under the gradient concentrations of LPS. In order to exclude the LPS-induced Nrf2 activation effects, cells pretreated with gradient concentration of LPS alone were used as the control. As shown in Fig. 4B, LPS-stimulation before drug exposure (200 nM) activated **pro2** and resulted in the LPS concentration-dependent enhancement of Nrf2-ARE inducing activity, while the potency of **2** and **3** did not show obvious changes. Under LPS stimulation, **pro2** showed the lowest EC_{50} value (0.32 μM) among them in the ARE induction activity (Fig. 4C). Together, the thiazolidinone-based prodrug **pro2** can be selectively activated by LPS-induced intracellular ROS, enhancing the Nrf2-ARE system at a much lower concentration than the parent drug.

3.5. Activation of the Nrf2-ARE regulated antioxidant system in the RAW264.7 cells

To ascertain the effects of **pro2** on the transcription of Nrf2-ARE-driven genes, the mRNA levels of Nrf2 downstream genes, Heme oxygenase 1 (*HO-1*), NAD(P)H: Quinone Oxidoreductase 1 (*NQO1*) and glutamate-cysteine ligase, modifier subunit *(GCLM)*, were examined (Fig. 5A–C). The quantitative real-time PCR (qRT-PCR) analysis showed that exposure of RAW264.7 cells to 20 ng/mL LPS for 8 h slightly increased the transcription of Nrf2 targeted genes. Addition of **pro2** (500 nM) highly enhanced the transcription, superior to the effects of **2** and its methyl ester prodrug at the same concentration. The protein levels of these genes were measured by immunostaining, and **pro2** remarkably accumulated Nrf2 protein and elevated downstream antioxidant enzymes, more potent than the parent drug and its methyl ester prodrug (Fig. 5D).

Subsequently, to explore the effects of **pro2** on antioxidant capacity under inflammatory conditions, the activities of representative enzymes, superoxide dismutase (SOD) and glutathione peroxidase (GSH-Px), were determined. Mouse RAW 264.7 cells treated with LPS (20 ng/mL) alone showed the obvious decrease in activities of SOD and GSH-Px (Fig. 5E and F). Treatment with **pro2** significantly restored the activities of SOD and GSH-Px, while the parent compound and its methyl ester analog were less efficient. We also measured the GSH/GSSG ratio and myeloperoxidase (MPO) activity (Fig. 5G and H), two important markers for indication of oxidative stress. LPS exposure caused huge decline in the GSH/GSSG ratio and sharp rise in the MPO activity, confirming that LPS could cause the oxidative stress. The addition of **pro2** restored the levels nearly back to normal, the parent drug and its methyl analog showed similar trend but much lower activity.

3.6. Anti-inflammatory effects of **pro2** in the LPS-induced RAW264.7 cells

Nrf2 activation has been proven to be an effective way to relieve the inflammatory conditions. We first examined the mRNA levels of IL-1β and IL-6, which can be transcriptionally repressed by Nrf2 [66]. After LPS (20 ng/mL) stimulation for 8 h, the mRNA levels of IL-1β and IL-6 were remarkably induced in the RAW264.7 cells. Treatment with **2** or the methyl ester prodrug **3** slightly inhibited the transcription of IL-1β and IL-6. Of note, treatment with **pro2** resulted in significant suppression effects (Fig. 6A and B). Consistent with the results of the PCR analyses, **2** and **3** showed moderate effects on the inhibition of LPS-induced elevation of IL-1β and IL-6 protein, but **pro2**, at the same concentration, almost completely suppressed the elevation (Fig. 6C). Then, we quantitatively evaluated several inflammatory mediators that are closely related with ROS, including IL-1β, IL-6, TNF-α and NO. As expected, all these inflammatory factors increased markedly in the LPS-treated groups, and **pro2** showed obvious superiority in the suppression of IL-1β, IL-6 and TNF-α production (Fig. 6D–F). The LPS triggered NO production was also remarkably diminished by **pro2** with an EC_{50} of 0.12 μM, while compound **2** and **3** showed higher EC_{50} values (Fig. 6G).

3.7. In vivo efficacy of **pro2** against the LPS-induced inflammatory conditions

After confirming the ROS-responsive Nrf2 activation effects of **pro2** in live cells, we finally investigated the therapeutic potential of **pro2** *in vivo*. To explore the suitability of thiazolidinone-based prodrug for oral administration, we evaluated the pharmacokinetics of **pro2** for both IV and PO, and the oral pharmacokinetics with bioavailability of 68.1% and half-life of 2.09 ± 0.93 h (Table 2) indicated **pro2** could be an effective oral medication.

Then, the murine LPS challenged acute inflammation model was used to evaluate anti-inflammation effects *in vivo*. C57BL/6 mice were challenged with LPS (300 μg/kg, IP) and then orally administrated with compound 4 h after the LPS challenge for 3 days. The blank group only received saline during the experiment. Dexamethasone (DXM), the widely used steroid anti-inflammatory drug, was used as the positive control. Animals were sacrificed 24 h after the last dose of compound and sera were collected. LPS challenge markedly elevated the pro-inflammatory cytokines in mice sera, including IL-1β, IL-6, TNF-α and IFN-γ. DXM treatment (10 mg/kg) diminished inflammatory response (Fig. 7A–D). Oral administration of **2** (40 mg/kg) showed moderate anti-inflammation activity, much less potent than DXM. **Pro2** showed comparable therapeutic effects with DXM at the same dose (10 mg/kg), and high dose of **pro2** showed more potent effects, indicating the dose-dependent behavior. Taken together, these results suggested that the thiazolidinone-based ROS-responsive prodrug of the Keap1-Nrf2 PPI inhibitor is an effective oral medication for oxidative stress related inflammatory conditions.

4. Conclusions

In this study, a new ROS-activated prodrug **pro2** was developed by utilizing H_2O_2-responsive thiazolidinone moiety to shield the key carboxyl pharmacophore in Keap1-Nrf2 inhibitor. Inflammation derived intracellular H_2O_2 can deprotect carboxyl group, producing the potent Keap1-Nrf2 inhibitor to selectively activate Nrf2-regulated antioxidant system in target cells. Moreover, the thiazolidinone modification of the carboxyl group improve the physicochemical properties and cell membrane permeability of the parent drug. Further cellular studies showed that **pro2** can stay inactive at physiological conditions and be much more potent than the parent drug at inflammatory conditions. In addition, thiazolidinone-based drug displayed good stabilities at various physiological conditions and appropriate PK profile for oral administration. Finally, *in vivo* therapeutic activity was demonstrated by oral use of **pro2** in LPS challenged acute inflammation model.

An increasing body of literature has revealed that over and unselective activation of Nrf2 may cause unexpected risks and particularly contribute to the initiation and progression of cancer [67–70], inspiring the discovery of precision Nrf2 activators. Direct Keap1-Nrf2 PPI inhibitors are assumed to have higher target selectivity than electrophilic Nrf2 activators. However, one critical challenge for the Keap1-Nrf2 inhibitors has also emerged. Direct Keap1-Nrf2 inhibitors are designed to bind to Keap1 with a similar pattern of Nrf2 ETGE motif, which may also affect functions of other Keap1 substrates with a similar recognition motif [71,72]. Developing Keap1-Nrf2 inhibitors selectively activating Nrf2 in specific pathologic conditions is a new avenue. The carboxyl group, the key pharmacophore in the direct Keap1-Nrf2 inhibitors, can be utilized to design a targeted prodrug that not only improves the ADMET properties but also selectively activates Nrf2. The high concentrations of H_2O_2 in the inflammatory environment can serve as the stimulus for prodrug activation. This pathologic site-selective drug delivery system therefore restricts the effects of Keap1-Nrf2 inhibitors on Keap1-involved interactome of normal tissues.

Taken together, our study confirmed that this H_2O_2-activated prodrug can achieve selective Nrf2 activation and enhanced *in vivo* efficacy simultaneously, providing an attractive approach for the further development of Keap1-Nrf2 inhibitors.

Declaration of competing interest

All authors have given approval to the final version of the manuscript. The authors have no conflicts of interest to declare.

Acknowledgments

This study was supported by Projects 81773639, 81773581, 81803363 and 81930100 of the National Natural Science Foundation of China; National Science & Technology Major Project 'Key New Drug Creation and Manufacturing Program', China (No: 2018ZX09711002 and 2017ZX09302003); the Priority Academic Program Development of Jiangsu Higher Education Institutions; China Postdoctoral Science Foundation-funded Project (2017M620231 and 2018T110576); CPU2018GY02 of Double First Class Innovation Team of China Pharmaceutical University; Program for Outstanding Scientific and Technological Innovation Team of Jiangsu Higher Education, Jiangsu Qing Lan Project and the Young Elite Scientists Sponsorship Program by CAST.

Appendix A. Supplementary data

Supplementary data to this article can be found online at https://doi.org/10.1016/j.redox.2020.101565.

Abbreviations

Nrf2	Nuclear factor erythroid 2-related factor 2
Keap1	Kelch-like ECH-associated protein 1
H_2O_2	hydrogen peroxide
ROS	reactive oxygen species
ARE	antioxidant response element
PPI	protein-protein interaction
ITC	Isothermal Titration Calorimetry
PAMPA	parallel artificial membrane permeability assay
Pe	permeability coefficients
LPS	lipopolysaccharide
HO-1	Heme oxygenase 1
NQO-1	NAD(P)H dehydrogenase (quinone) 1
GCLM	glutamate-cysteine ligase regulatory subunit
qRT-PCR	quantitative real-time PCR
SOD	superoxide dismutase

GPx	glutathione peroxidase
MPO	myeloperoxidase
DXM	dexamethasone

References

[1] L.E. Tebay, H. Robertson, S.T. Durant, S.R. Vitale, T.M. Penning, A.T. Dinkova-Kostova, J.D. Hayes, Mechanisms of activation of the transcription factor Nrf2 by redox stressors, nutrient cues, and energy status and the pathways through which it attenuates degenerative disease, Free Radic. Biol. Med. 88 (Pt B) (2015) 108–146.

[2] C. Tonelli, I.I.C. Chio, D.A. Tuveson, Transcriptional regulation by Nrf2, Antioxidants Redox Signal. 29 (17) (2018) 1727–1745.

[3] A. Cuadrado, G. Manda, A. Hassan, M.J. Alcaraz, C. Barbas, A. Daiber, P. Ghezzi, R. Leon, M.G. Lopez, B. Oliva, M. Pajares, A.I. Rojo, N. Robledinos-Anton, A.M. Valverde, E. Guney, H. Schmidt, Transcription factor NRF2 as a therapeutic target for chronic diseases: a systems medicine approach, Pharmacol. Rev. 70 (2) (2018) 348–383.

[4] T. Suzuki, M. Yamamoto, Stress-sensing mechanisms and the physiological roles of the Keap1-Nrf2 system during cellular stress, J. Biol. Chem. 292 (41) (2017) 16817–16824.

[5] D.A. Abed, M. Goldstein, H. Albanyan, H. Jin, L. Hu, Discovery of direct inhibitors of Keap1-Nrf2 protein-protein interaction as potential therapeutic and preventive agents, Acta Pharm. Sin. B 5 (4) (2015) 285–299.

[6] M.-C. Lu, J.-A. Ji, Z.-Y. Jiang, Q.-D. You, The keap1–Nrf2–ARE pathway as a potential preventive and therapeutic target: an update, Med. Res. Rev. 36 (5) (2016) 924–963.

[7] M. Yamamoto, T.W. Kensler, H. Motohashi, The KEAP1-NRF2 system: a thiol-based sensor-effector apparatus for maintaining redox homeostasis, Physiol. Rev. 98 (3) (2018) 1169–1203.

[8] N. Keleku-Lukwete, M. Suzuki, M. Yamamoto, An overview of the advantages of KEAP1-NRF2 system activation during inflammatory disease treatment, Antioxidants Redox Signal. 29 (17) (2018) 1746–1755.

[9] A. Cuadrado, A.I. Rojo, G. Wells, J.D. Hayes, S.P. Cousin, W.L. Rumsey, O.C. Attucks, S. Franklin, A.L. Levonen, T.W. Kensler, A.T. Dinkova-Kostova, Therapeutic targeting of the NRF2 and KEAP1 partnership in chronic diseases, Nat. Rev. Drug Discov. 18 (4) (2019) 295–317.

[10] H. Zhou, Y. Wang, Q. You, Z. Jiang, Recent progress in the development of small molecule Nrf2 activators: a patent review (2017-present), Expert Opin. Ther. Pat. 30 (3) (2020) 209–225.

[11] T.G. Davies, W.E. Wixted, J.E. Coyle, C. Griffiths-Jones, K. Hearn, R. McMenamin, D. Norton, S.J. Rich, C. Richardson, G. Saxty, H.M.G. Willems, A.J.A. Woolford, J.E. Cottom, J.-P. Kou, J.G. Yonchuk, H.G. Feldser, Y. Sanchez, J.P. Foley, B.J. Bolognese, G. Logan, P.L. Podolin, H. Yan, J.F. Callahan, T.D. Heightman, J.K. Kerns, Monoacidic inhibitors of the kelch-like ECH-associated protein 1: nuclear factor erythroid 2-related factor 2 (KEAP1:NRF2) protein–protein interaction with high cell potency identified by fragment-based discovery, J. Med. Chem. 59 (8) (2016) 3991–4006.

[12] T.D. Heightman, J.F. Callahan, E. Chiarparin, J.E. Coyle, C. Griffiths-Jones, A.S. Lakdawala, R. McMenamin, P.N. Mortenson, D. Norton, T.M. Peakman, S.J. Rich, C. Richardson, W.L. Rumsey, Y. Sanchez, G. Saxty, H.M.G. Willems, L. Wolfe 3rd, A.J. Woolford, Z. Wu, H. Yan, J.K. Kerns, T.G. Davies, Structure-activity and structure-conformation relationships of aryl propionic acid inhibitors of the kelch-like ECH-associated protein 1/nuclear factor erythroid 2-related factor 2 (KEAP1/NRF2) protein-protein interaction, J. Med. Chem. 62 (9) (2019) 4683–4702.

[13] P.R. Lazzara, B.P. David, A. Ankireddy, B. Richardson, K. Dye, K.M. Ratia, S.P. Reddy, T.W. Moore, Isoquinoline kelch-like ECH-associated protein 1-nuclear factor (Erythroid-derived 2)-like 2 (KEAP1-NRF2) inhibitors with high metabolic stability, J. Med. Chem. (2019), https://doi.org/10.1021/acs.jmedchem.9b01074.

[14] C.S. Jiang, C.L. Zhuang, K. Zhu, J. Zhang, L.A. Muehlmann, J.P. Figueiro Longo, R.B. Azevedo, W. Zhang, N. Meng, H. Zhang, Identification of a novel small-molecule Keap1-Nrf2 PPI inhibitor with cytoprotective effects on LPS-induced cardiomyopathy, J. Enzym. Inhib. Med. Chem. 33 (1) (2018) 833–841.

[15] B. Ma, B. Lucas, A. Capacci, E.Y. Lin, J.H. Jones, M. Dechantsreiter, I. Enyedy, D. Marcotte, G. Xiao, B. Li, K. Richter, Design, synthesis and identification of novel, orally bioavailable non-covalent Nrf2 activators, Bioorg. Med. Chem. Lett 30 (4) (2020) 126852.

[16] D.A. Abed, S. Lee, L. Hu, Discovery of disubstituted xylylene derivatives as small molecule direct inhibitors of Keap1-Nrf2 protein-protein interaction, Bioorg. Med. Chem. 28 (6) (2020) 115343.

[17] N. Meng, H. Tang, H. Zhang, C. Jiang, L. Su, X. Min, W. Zhang, H. Zhang, Z. Miao, W. Zhang, C. Zhuang, Fragment-growing guided design of Keap1-Nrf2 protein-protein interaction inhibitors for targeting myocarditis, Free Radic. Biol. Med. 117 (2018) 228–237.

[18] Z. Jiang, M. Lu, Q.D. You, Discovery and development of kelch-like ECH-associated protein 1: nuclear factor erythroid 2-related factor 2 (KEAP1:NRF2) protein-protein interaction inhibitors: achievements, challenges and future directions, J. Med. Chem. 59 (24) (2016) 10837–10858.

[19] J.S. Pallesen, K.T. Tran, A. Bach, Non-covalent small-molecule kelch-like ECH-associated protein 1-nuclear factor erythroid 2-related factor 2 (Keap1-Nrf2) inhibitors and their potential for targeting central nervous system diseases, J. Med. Chem. 61 (18) (2018) 8088–8103.

[20] C. Zhuang, Z. Wu, C. Xing, Z. Miao, Small molecules inhibiting Keap1-Nrf2 protein-protein interactions: a novel approach to activate Nrf2 function, MedChemComm 8 (2) (2017) 286–294.

[21] G.M. DeNicola, F.A. Karreth, T.J. Humpton, A. Gopinathan, C. Wei, K. Frese, D. Mangal, K.H. Yu, C.J. Yeo, E.S. Calhoun, F. Scrimieri, J.M. Winter, R.H. Hruban, C. Iacobuzio-Donahue, S.E. Kern, I.A. Blair, D.A. Tuveson, Oncogene-induced Nrf2 transcription promotes ROS detoxification and tumorigenesis, Nature 475 (7354) (2011) 106–109.

[22] L. Lignitto, S.E. LeBoeuf, H. Homer, S. Jiang, M. Askenazi, T.R. Karakousi, H.I. Pass, A.J. Bhutkar, A. Tsirigos, B. Ueberheide, V.I. Sayin, T. Papagiannakopoulos, M. Pagano, Nrf2 activation promotes lung cancer metastasis by inhibiting the degradation of Bach1, Cell 178 (2) (2019) 316–329 e18.

[23] Z.Y. Jiang, M.C. Lu, Q.D. You, Nuclear factor erythroid 2-related factor 2 (Nrf2) inhibition: an emerging strategy in cancer therapy, J. Med. Chem. 62 (8) (2019) 3840–3856.

[24] M. Rojo de la Vega, E. Chapman, D.D. Zhang, NRF2 and the hallmarks of cancer, Canc. Cell 34 (1) (2018) 21–43.

[25] N. Robledinos-Anton, R. Fernandez-Gines, G. Manda, A. Cuadrado, Activators and inhibitors of NRF2: a review of their potential for clinical development, Oxid. Med. Cell. Longev. 2019 (2019) 9372182.

[26] S. Menegon, A. Columbano, S. Giordano, The dual roles of NRF2 in cancer, Trends Mol. Med. 22 (7) (2016) 578–593.

[27] P. Zavattari, A. Perra, S. Menegon, M.A. Kowalik, A. Petrelli, M.M. Angioni, A. Follenzi, L. Quagliata, G.M. Ledda-Columbano, L. Terracciano, S. Giordano, A. Columbano, Nrf2, but not beta-catenin, mutation represents an early event in rat hepatocarcinogenesis, Hepatology 62 (3) (2015) 851–862.

[28] C. Orru, M. Szydlowska, K. Taguchi, P. Zavattari, A. Perra, M. Yamamoto, A. Columbano, Genetic inactivation of Nrf2 prevents clonal expansion of initiated cells in a nutritional model of rat hepatocarcinogenesis, J. Hepatol. 69 (3) (2018) 635–643.

[29] J.R. Stone, S. Yang, Hydrogen peroxide: a signaling messenger, Antioxidants Redox Signal. 8 (3–4) (2006) 243–270.

[30] R. Radi, Oxygen radicals, nitric oxide, and peroxynitrite: redox pathways in molecular medicine, Proc. Natl. Acad. Sci. U. S. A 115 (23) (2018) 5839–5848.

[31] H. Sies, Hydrogen peroxide as a central redox signaling molecule in physiological oxidative stress: oxidative eustress, Redox Biol. 11 (2017) 613–619.

[32] B. D'Autreaux, M.B. Toledano, ROS as signalling molecules: mechanisms that generate specificity in ROS homeostasis, Nat. Rev. Mol. Cell Biol. 8 (10) (2007) 813–824.

[33] E.A. Veal, A.M. Day, B.A. Morgan, Hydrogen peroxide sensing and signaling, Mol. Cell 26 (1) (2007) 1–14.

[34] M. Mittal, M.R. Siddiqui, K. Tran, S.P. Reddy, A.B. Malik, Reactive oxygen species in inflammation and tissue injury, Antioxidants Redox Signal. 20 (7) (2014) 1126–1167.

[35] K.J. Barnham, C.L. Masters, A.I. Bush, Neurodegenerative diseases and oxidative stress, Nat. Rev. Drug Discov. 3 (3) (2004) 205–214.

[36] S. Reuter, S.C. Gupta, M.M. Chaturvedi, B.B. Aggarwal, Oxidative stress, inflammation, and cancer: how are they linked? Free Radic. Biol. Med. 49 (11) (2010) 1603–1616.

[37] R. Weinstain, E.N. Savariar, C.N. Felsen, R.Y. Tsien, In vivo targeting of hydrogen peroxide by activatable cell-penetrating peptides, J. Am. Chem. Soc. 136 (3) (2014) 874–877.

[38] M.C. Chang, A. Pralle, E.Y. Isacoff, C.J. Chang, A selective, cell-permeable optical probe for hydrogen peroxide in living cells, J. Am. Chem. Soc. 126 (47) (2004) 15392–15393.

[39] E.W. Miller, A.E. Albers, A. Pralle, E.Y. Isacoff, C.J. Chang, Boronate-based fluorescent probes for imaging cellular hydrogen peroxide, J. Am. Chem. Soc. 127 (47) (2005) 16652–16659.

[40] G.C. Van de Bittner, E.A. Dubikovskaya, C.R. Bertozzi, C.J. Chang, In vivo imaging of hydrogen peroxide production in a murine tumor model with a chemoselective bioluminescent reporter, Proc. Natl. Acad. Sci. U. S. A 107 (50) (2010) 21316–21321.

[41] B.C. Dickinson, C.J. Chang, Chemistry and biology of reactive oxygen species in signaling or stress responses, Nat. Chem. Biol. 7 (8) (2011) 504–511.

[42] H. Hagen, P. Marzenell, E. Jentzsch, F. Wenz, M.R. Veldwijk, A. Mokhir, Aminoferrocene-based prodrugs activated by reactive oxygen species, J. Med. Chem. 55 (2) (2012) 924–934.

[43] L. Yuan, W. Lin, Y. Xie, B. Chen, S. Zhu, Single fluorescent probe responds to H2O2, NO, and H2O2/NO with three different sets of fluorescence signals, J. Am. Chem. Soc. 134 (2) (2012) 1305–1315.

[44] J.L. Kolanowski, A. Kaur, E.J. New, Selective and reversible approaches toward imaging redox signaling using small-molecule probes, Antioxidants Redox Signal. 24 (13) (2016) 713–730.

[45] L. Wu, A.C. Sedgwick, X. Sun, S.D. Bull, X.P. He, T.D. James, Reaction-based fluorescent probes for the detection and imaging of reactive oxygen, nitrogen, and sulfur species, Acc. Chem. Res. 52 (9) (2019) 2582–2597.

[46] Y. Kuang, K. Balakrishnan, V. Gandhi, X. Peng, Hydrogen peroxide inducible DNA cross-linking agents: targeted anticancer prodrugs, J. Am. Chem. Soc. 133 (48) (2011) 19278–19281.

[47] E.J. Kim, S. Bhuniya, H. Lee, H.M. Kim, C. Cheong, S. Maiti, K.S. Hong, J.S. Kim, An activatable prodrug for the treatment of metastatic tumors, J. Am. Chem. Soc. 136 (39) (2014) 13888–13894.

[48] S. Daum, V.F. Chekhun, I.N. Todor, N.Y. Lukianova, Y.V. Shvets, L. Sellner, K. Putzker, J. Lewis, T. Zenz, I.A. de Graaf, G.M. Groothuis, A. Casini, O. Zozulia, F. Hampel, A. Mokhir, Improved synthesis of N-benzylaminoferrocene-based prodrugs and evaluation of their toxicity and antileukemic activity, J. Med. Chem. 58 (4) (2015) 2015–2024.

[49] S. Daum, M.S.V. Reshetnikov, M. Sisa, T. Dumych, M.D. Lootsik, R. Bilyy, E. Bila,

C. Janko, C. Alexiou, M. Herrmann, L. Sellner, A. Mokhir, Lysosome-targeting amplifiers of reactive oxygen species as anticancer prodrugs, Angew. Chem., Int. Ed. Engl. 56 (49) (2017) 15545–15549.
[50] W. Chen, H. Fan, K. Balakrishnan, Y. Wang, H. Sun, Y. Fan, V. Gandhi, L.A. Arnold, X. Peng, Discovery and optimization of novel hydrogen peroxide activated aromatic nitrogen mustard derivatives as highly potent anticancer agents, J. Med. Chem. 61 (20) (2018) 9132–9145.
[51] V. Reshetnikov, S. Daum, C. Janko, W. Karawacka, R. Tietze, C. Alexiou, S. Paryzhak, T. Dumych, R. Bilyy, P. Tripal, B. Schmid, R. Palmisano, A. Mokhir, ROS-responsive N-alkylaminoferrocenes for cancer-cell-specific targeting of mitochondria, Angew. Chem., Int. Ed. Engl. 57 (37) (2018) 11943–11946.
[52] S. Wang, G. Yu, Z. Wang, O. Jacobson, L.S. Lin, W. Yang, H. Deng, Z. He, Y. Liu, Z.Y. Chen, X. Chen, Enhanced antitumor efficacy by a cascade of reactive oxygen species generation and drug release, Angew. Chem., Int. Ed. Engl. 58 (41) (2019) 14758–14763.
[53] T. Meng, J. Han, P. Zhang, J. Hu, J. Fu, J. Yin, Introduction of the α-ketoamide structure: en route to develop hydrogen peroxide responsive prodrugs, Chem. Sci. 10 (30) (2019) 7156–7162.
[54] J. Peiro Cadahia, J. Bondebjerg, C.A. Hansen, V. Previtali, A.E. Hansen, T.L. Andresen, M.H. Clausen, Synthesis and evaluation of hydrogen peroxide sensitive prodrugs of methotrexate and aminopterin for the treatment of rheumatoid arthritis, J. Med. Chem. 61 (8) (2018) 3503–3515.
[55] N.S. Andersen, J. Peiro Cadahia, V. Previtali, J. Bondebjerg, C.A. Hansen, A.E. Hansen, T.L. Andresen, M.H. Clausen, Methotrexate prodrugs sensitive to reactive oxygen species for the improved treatment of rheumatoid arthritis, Eur. J. Med. Chem. 156 (2018) 738–746.
[56] Y. Zhao, Matthew M. Cerda, M.D. Pluth, Fluorogenic hydrogen sulfide (H2S) donors based on sulfenyl thiocarbonates enable H2S tracking and quantification, Chem. Sci. 10 (6) (2019) 1873–1878.
[57] Y. Zhao, M.D. Pluth, Hydrogen sulfide donors activated by reactive oxygen species, Angew. Chem. Int. Ed. 55 (47) (2016) 14638–14642.
[58] Y. Li, Y. Shu, M. Liang, X. Xie, X. Jiao, X. Wang, B. Tang, A two-photon H2 O2 -activated CO photoreleaser, Angew. Chem., Int. Ed. Engl. 57 (38) (2018) 12415–12419.
[59] T.T. Hoang, T.P. Smith, R.T. Raines, A boronic acid conjugate of angiogenin that shows ROS-responsive neuroprotective activity, Angew. Chem. 129 (10) (2017) 2663–2666.
[60] Z.Y. Jiang, L.L. Xu, M.C. Lu, Z.Y. Chen, Z.W. Yuan, X.L. Xu, X.K. Guo, X.J. Zhang, H.P. Sun, Q.D. You, Structure-activity and structure-property relationship and exploratory in vivo evaluation of the nanomolar keap1-Nrf2 protein-protein interaction inhibitor, J. Med. Chem. 58 (16) (2015) 6410–6421.
[61] Z.-Y. Jiang, M.-C. Lu, L.L. Xu, T.-T. Yang, M.-Y. Xi, X.-L. Xu, X.-K. Guo, X.-J. Zhang, Q.-D. You, H.-P. Sun, Discovery of potent keap1–Nrf2 protein–protein interaction inhibitor based on molecular binding determinants analysis, J. Med. Chem. 57 (6) (2014) 2736–2745.
[62] A.D. Jain, H. Potteti, B.G. Richardson, L. Kingsley, J.P. Luciano, A.F. Ryuzoji, H. Lee, A. Krunic, A.D. Mesecar, S.P. Reddy, T.W. Moore, Probing the structural requirements of non-electrophilic naphthalene-based Nrf2 activators, Eur. J. Med. Chem. 103 (2015) 252–268.
[63] K.T. Tran, J.S. Pallesen, S.M.O. Solbak, D. Narayanan, A. Baig, J. Zang, A. Aguayo-Orozco, R.M.C. Carmona, A.D. Garcia, A. Bach, A comparative assessment study of known small-molecule keap1-Nrf2 protein-protein interaction inhibitors: chemical synthesis, binding properties, and cellular activity, J. Med. Chem. 62 (17) (2019) 8028–8052.
[64] M.C. Lu, J. Zhao, Y.T. Liu, T. Liu, M.M. Tao, Q.D. You, Z.Y. Jiang, CPUY192018, a potent inhibitor of the Keap1-Nrf2 protein-protein interaction, alleviates renal inflammation in mice by restricting oxidative stress and NF-kappaB activation, Redox Biol. 26 (2019) 101266.
[65] C. Perez, J.-P. Monserrat, Y. Chen, S.M. Cohen, Exploring hydrogen peroxide responsive thiazolidinone-based prodrugs, Chem. Commun. 51 (33) (2015) 7116–7119.
[66] E.H. Kobayashi, T. Suzuki, R. Funayama, T. Nagashima, M. Hayashi, H. Sekine, N. Tanaka, T. Moriguchi, H. Motohashi, K. Nakayama, M. Yamamoto, Nrf2 suppresses macrophage inflammatory response by blocking proinflammatory cytokine transcription, Nat. Commun. 7 (2016) 11624.
[67] S. Mukhopadhyay, D. Goswami, P.P. Adiseshaiah, W. Burgan, M. Yi, T.M. Guerin, S.V. Kozlov, D.V. Nissley, F. McCormick, Undermining glutaminolysis bolsters chemotherapy while NRF2 promotes chemoresistance in KRAS-driven pancreatic cancers, Canc. Res. 80 (8) (2020) 1630–1643.
[68] M.H. Bailey, C. Tokheim, E. Porta-Pardo, S. Sengupta, D. Bertrand, A. Weerasinghe, A. Colaprico, M.C. Wendl, J. Kim, B. Reardon, P.K. Ng, K.J. Jeong, S. Cao, Z. Wang, J. Gao, Q. Gao, F. Wang, E.M. Liu, L. Mularoni, C. Rubio-Perez, N. Nagarajan, I. Cortes-Ciriano, D.C. Zhou, W.W. Liang, J.M. Hess, V.D. Yellapantula, D. Tamborero, A. Gonzalez-Perez, C. Suphavilai, J.Y. Ko, E. Khurana, P.J. Park, E.M. Van Allen, H. Liang, M.C.W. Group, N. Cancer Genome Atlas Research, M.S. Lawrence, A. Godzik, N. Lopez-Bigas, J. Stuart, D. Wheeler, G. Getz, K. Chen, A.J. Lazar, G.B. Mills, R. Karchin, L. Ding, Comprehensive characterization of cancer driver genes and mutations, Cell 173 (2) (2018) 371–385 e18.
[69] E.W. Cloer, D. Goldfarb, T.P. Schrank, B.E. Weissman, M.B. Major, NRF2 activation in cancer: from DNA to protein, Canc. Res. 79 (5) (2019) 889–898.
[70] L. Lignitto, S.E. LeBoeuf, H. Homer, S. Jiang, M. Askenazi, T.R. Karakousi, H.I. Pass, A.J. Bhutkar, A. Tsirigos, B. Ueberheide, V.I. Sayin, T. Papagiannakopoulos, M. Pagano, Nrf2 activation promotes lung cancer metastasis by inhibiting the degradation of Bach1, Cell 178 (2) (2019) 316–329.
[71] Y. Zhang, Z. Shi, Y. Zhou, Q. Xiao, H. Wang, Y. Peng, Emerging substrate proteins of kelch-like ECH associated protein 1 (Keap1) and potential challenges for the development of small-molecule inhibitors of the keap1-nuclear factor erythroid 2-related factor 2 (Nrf2) protein-protein interaction, J. Med. Chem. (2020), https://doi.org/10.1021/acs.jmedchem.9b01865.
[72] A. Kopacz, D. Kloska, H.J. Forman, A. Jozkowicz, A. Grochot-Przeczek, Beyond repression of Nrf2: an update on Keap1, Free Radical Biol. Med. (2020), https://doi.org/10.1016/j.freeradbiomed.2020.03.023.